RI 8950

Rock Stability Analysis Using Acoustic Spectroscopy

By D. R. Hanson

UNITED STATES DEPARTMENT OF THE INTERIOR

Rock Stability Analysis Using Acoustic Spectroscopy

By D. R. Hanson

UNITED STATES DEPARTMENT OF THE INTERIOR
Donald Paul Hodel, Secretary

BUREAU OF MINES
Robert C. Horton, Director

CONTENTS

ILLUSTRATIONS

ILLUSTRATIONS--Continued

TABLES

UNIT OF MEASURE ABBREVIATIONS USED IN THIS REPORT

cm	centimeter	μF	microfarad
dB	decibel	MΩ	megohm
ft^3	cubic foot	mm	millimeter
Hz	hertz	ms	millisecond
kHz	kilohertz	N	newton
kN	kilonewton	Ω	ohm
kΩ	kilohm	pF	picofarad
lb	pound	V	volt
m	meter	W	watt
mA	milliampere		

ROCK STABILITY ANALYSIS USING ACOUSTIC SPECTROSCOPY

By D. R. Hanson[1]

ABSTRACT

This Bureau of Mines study examines the acoustic vibrational spectra of rock slabs in the range of 0 to 5,000 Hz. The power spectra of so-called drummy rocks were found to be diagnostically enhanced in the range of 200 to 1,000 Hz. Comparison of the power in this band with that in a band from 3,000 to 3,500 Hz provides a quantitative measure of rock stability.

A prototype field instrument was designed, constructed, and field-tested. This battery-powered instrument computes the power contained in the two frequency bands mentioned, compares the magnitude of these two quantities, and displays a number that is related to the detachment of the block tested. Field tests show that this instrument is capable of giving reliable measurements of block stability under conditions of noise and dust that would seriously degrade the accuracy of normal sounding techniques.

---

[1]Mining engineer, Denver Research Center, Bureau of Mines, Denver, CO.

INTRODUCTION

In 1979 and 1980, 98 fatalities (1-2)[2] and 2,344 injury accidents (3-4) were caused in underground coal mines by falls of roof, rib, or face. The time-honored method of testing for roof stability is to tap the block in question with a "scaling" or "sounding" bar and listen to the "drumminess" of the rock. Based on a miner's experience and specific conditions of the mine itself, a judgment is made as to the stability of the slab. The drummier or lower pitched the detected sound, the less stable the rock is judged to be. While this method is usually quite effective, it is also rather subjective in nature, and errors can be made in judging rock stability. Factors such as inexperience, inability to hear the rock response, the miner's health, nearby loud equipment, obscuring dust, and simple human carelessness tend to degrade the ability to distinquish between stable and unstable blocks. Experience plays perhaps the major role, as most miners killed or injured are less than 30 years old and have been on the job 5 years or less (1-3).

The goal of this Bureau of Mines study is to find a method of sounding that will give a rapid, objective, and reliable measure of block stability. Several criteria were set up to guide technique choice and instrumentation design. Paramount of these were convenience and simplicity. To gain miner acceptance, any instrumentation must be simple to operate, reliable, and rugged. In addition, it must be usable on any slab without special surface preparation. Finally, the technique must be able to give rapid measurements of local rock conditions without requiring extensive, sophisticated support equipment.

Preliminary investigations were made on possible testing methods, including low-frequency acoustic sounding, ultrasonic acoustic sounding, radar probing, and high resolution resistivity. Based on the criteria outlined above, the technique judged to have the highest probability of success was low-frequency acoustic testing.

ACKNOWLEDGMENTS

ACOUSTIC BEHAVIOR OF DECOUPLED ROCK SLABS

Numerous attempts have been made to develop, on both a theoretical and empirical basis, an objective method to predict the behavior of rock slabs as they become decoupled from their surroundings. One of the earlier attempts to quantify the spectral response of impacted roof slabs was made by Summerfield (5). Briefly, Summerfield found that when rocks were struck with a hammer or sounding bar, drummy rocks vibrated at lower frequencies and for a longer time than did solid rocks. This variation in dynamic response was proposed as a means of discriminating between the two types of rocks. In 1974, the French (6) reported the development of an instrument that gave a numerical measure of rock conditions based on vibrational behavior. However, this research effort was later abandoned. More recently, Palmer and Czirr (7) examined the vibrational

---

[2]Underlined numbers in parentheses refer to items in the list of references preceding the appendixes.

behavior of coal mine roofs and observed the same sort of behavior as had Summerfield. That is, solid rocks tended to have a broadband, noiselike spectrum. With increasing drumminess, this changed to spiky line spectra enchanced in the frequency range of 0 to 1,000 Hz.

A theoretical explanation of this behavior may be obtained by examining the normal mode response of a rock modeled as a lumped parameter, mechanical system. While all real structures are continuous systems and are not composed of lumped masses, it is instructive to analyze them as such to obtain a feeling for their general behavior. Over a wide range of frequencies, crystalline rocks have been observed to behave as Voigt or Kelvin solids (8). This means that each mass can be viewed as coupled to its surroundings by a parallel combination of springs and dashpots. The equation of motion for such a system in free vibration is

$$[m] \{\ddot{x}\} + [c] \{\dot{x}\}$$

$$+ [k] \{x\} = 0, \qquad (1)$$

where $[m] = m_{ij}$ = normalized inertia matrix,

$[c] = c_{ij}$ = normalized damping or friction matrix,

$[k] = k_{ij}$ = normalized stiffness matrix,

$\{x\}$ = matrix of normalized coordinates,

and $\{\dot{\ }\}$ = differentiation with respect to time.

The Q of a mechanical system is defined as the ratio of the peak energy in a cycle to the energy dissipated and so is a measurement of the damping present. If a system is first considered with very high Q or very low damping ($[c]$ approaches $[0]$), equation 1 reduces to

$$[m] \{\ddot{x}\} + [k] \{x\} = 0.$$

If motion is considered to be periodic, as

$$\{x\} = \{\lambda\}\ e^{i\omega t}, \qquad (1a)$$

where $\{\lambda\}$ = matrix of eigenvectors,

ω = angular frequency,

and t = time,

then $\omega_i^2 [m] \{\lambda\} = [k] \{\lambda\}.$

This relation has meaningful solutions only if

$$\text{Det } \{[k] - \omega_i^2 [m]\} = 0, \qquad (2)$$

from which the resonant frequencies, ω_i, may be computed.

Siggins and Enever (9) and Allison and Lama (10) have shown how a decrease in the stiffness matrix, Δk, will lower the resonant frequencies of the system. This stiffness reduction corresponds to a decoupling of the system from its surroundings. The matrices introduced here are assumed to be in a normalized coordinate system, which diagonalizes the matrices and decouples the resonant modes. With the modes decoupled, it is possible to examine the effect of Δk on a single mode. The first resonant frequency in the unmodified system is given by

$$k_1^2 - \omega_1^2\ m_1 = 0;$$

$$\omega_1 = \left(\frac{k_1}{m_1}\right)^{1/2} . \qquad (3)$$

When a Δk is introduced, equation 1 becomes

$$[k] \{\lambda\} - [\Delta k] \{\lambda\}$$

$$- \omega_{1M}^2 [m] \{\lambda\} = 0, \qquad (4)$$

which can be solved for the modified resonant frequencies, ω_{1M}, by

$$\text{Det } \{[k] - [\Delta k] - \omega_{1M}^2 [m]\} = 0. \qquad (5)$$

For the first resonance of the modified system,

$$k_1 - \Delta k_1 - \omega_{1M}^2 m_1 = 0;$$

$$\omega_{1M} = \left(\frac{k_1 - \Delta k_1}{m_1}\right)^{1/2} < \omega_1 = \left(\frac{k_1}{m_1}\right)^{1/2}. \quad (6)$$

This shows that for any given rock slab, a reduction in the stiffness of the system will result in a lowering of the system's resonant frequencies. Hence, enhanced low-frequency components in a given rock indicate decreased coupling and increased instability. This behavior provides the basis of stability measurements founded on spectral analysis of rock vibration.

If damping is now reintroduced and the system is assumed underdamped, the normalized coordinates $\{x\}$ may be written as

$$\{x\} = \{\lambda\} \exp[a_{ij} t], \quad (7)$$

which by substituting into equation 1 gives

$$a_{ij}^2 [m] \{\lambda\} + a_{ij} [c] \{\lambda\} + [k] \{\lambda\} = 0.$$

Looking only at the first mode,

$$a_{11} = -\left(\frac{c_1}{2m_1}\right) \pm \left(\frac{c_1}{2m_1} - \frac{k_1}{m_1}\right)^{1/2}$$

$$= \omega_1 [-\zeta_1 \pm (\zeta_1^2 - 1)^{1/2}],$$

where $\omega_1 = \left(\frac{k_1}{m_1}\right)^{1/2}$,

$$c_c = 2 (k_1 m_1)^{1/2},$$

and $\zeta_1 = \frac{c_1}{c_c}$.

For $\zeta < 1$ (underdamped mode),

$$x_1 = \lambda_1 e^{a_{11} t}$$

$$= \lambda_1 e^{\omega_1 [-\zeta_1 \pm (1 - \zeta_1^2)^{1/2}] t}, \quad (9)$$

which is a harmonic disturbance decaying at an exponential rate. When damping (ζ) is eliminated, this expression reverts to

Solving for a_{ij} in a normalized coordinate system,

$$\text{Det} \left[a_{ij}^2 [m] + a_{ij} [c] + [k] \right] = 0; \quad (8)$$

$$\begin{vmatrix} a_{11}^2 m_1 + a_{11} c_1 + k_1 & 0 & 0 & \cdots & 0 \\ 0 & a_{22}^2 m_2 + a_{22} c_2 + k_2 & & & \cdot \\ & & & \cdot & \\ \cdot & 0 & \cdot & & \\ & & \cdot & & \\ 0 & \cdots & \cdots & \cdot & a_{nn}^2 m_n + a_{nn} c_n + k_n \end{vmatrix} = 0.$$

equation 1a. If the amplitudes of successive maxima of equation 9 are x_0 and x, the log decrement is defined as the log of the ratio of these maxima, or

$$\delta = \log\left(\frac{x_0}{x_1}\right) = \frac{2\pi\zeta}{(1-\zeta^2)^{1/2}}. \qquad (10)$$

This expression gives a measure of how rapidly motion dies out as a function of the damping coefficient ζ, and can be related to the Q or sharpness of resonance of rock materials (8, 11) by

$$\delta = \frac{2\pi\zeta}{(1-\zeta^2)^{1/2}} = \frac{\pi}{Q},$$

or

$$Q = \frac{(1-\zeta^2)}{2\zeta}. \qquad (11)$$

Figure 1 (12) shows the effect of increased damping on amplitude of vibration versus excitation frequency. From this figure it can be seen that for any particular mode, increased damping will reduce the overall amplitude of the resonant peak, broaden the peak, and shift the maximum amplitude slightly lower in frequency. The amount of this frequency shift can be found (12) from

$$\frac{\omega_p}{\omega_n} = (1 - 2\zeta^2)^{1/2}, \qquad (12)$$

where ω_p = frequency with maximum amplitude,

and ω_n = undamped resonant frequency.

If a rock slab is viewed as a linear Rayleigh system (12) of n degrees of freedom, normal modes may be decoupled from one another. Individual mode responses may be superimposed and the
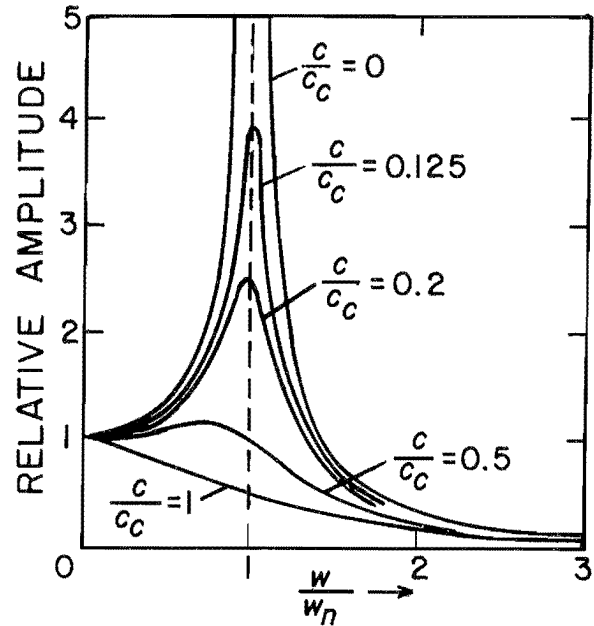
FIGURE 1. - Amplitude response of a single degree of freedom system with varying degrees of damping (from Seireg (12, p. 227)).

resonant behavior of the slab described by equations 1, 9, 10, 11, and 12. From these, a general pattern of behavior for unstable rock masses may be described. For a lightly damped, high-Q system, resonances will be shifted to lower frequencies as the rock is decoupled from its surroundings. Thus, a dominance of lower frequency components indicates a relatively more unstable block. As damping is increased, the amplitude differences between resonant and nonresonant frequencies will be reduced and discrimination based on the relative amplitude of spectral components degraded. It must be emphasized that although exact resonant frequencies and amplitudes will be highly dependent on the individual rocks and the input forcing functions, the general behavior described here should be observable.

EMPIRICAL TESTING

LABORATORY TESTING

To determine the modal behavior of rocks with increasing coupling, cubic rock samples were stressed uniaxially in a material testing machine with a capacity of 1.78×10^6 N. Samples of slate (15-cm cube), charcoal gray granite (25-

cm cube), and oil shale (18-cm cube) were ground smooth on all faces. A Dunegan/Endevco[3] model 2219E accelerometer was fastened to one face with phenyl salicylate. The accelerometer output was directed into a line-drive preamplifier (+20 dB amplification), another amplifier (-10 dB), and one channel of a fast Fourier transform (FFT) analyzer. Impacts were made with a hammer instrumented with a force transducer. The force transducer output was fed sequentially to an amplifier (-30 dB) and the other channel of the FFT analyzer. Figure 2 shows a block diagram of the experimental setup. Hammer blows were made at a distance of 5 to 10 cm from the accelerometer.

Power spectra for the force transducer and accelerometer, and the inertance function (output acceleration divided by input force), were computed for samples as they were loaded from 0 N to 26.7 kN (53.4 kN for the granite sample) in steps of 8.9 kN (2,000 lb). Typical results at 0 N are shown in figures 3 to 5 for an oil shale sample. Figure 3 is the amplitude spectrum of the input force and shows a smoothly varying amplitude, with most power concentrated below 3 kHz. Figure 4, the accelerometer spectrum, shows a similar behavior up to 4 kHz, after which a number of resonances appear. The inertance (fig. 5) is broken into a series of peaks and nodes, except for the region from 0 to 3 kHz. This general behavior was observed for all samples at 0 N applied static force. In contrast are figures 6 through 8, which were made at 17.8 kN (4,000 lb) applied force. The impact spectrum (fig. 6) is basically identical to that at 0 N, but the accelerometer spectrum and inertance (figs. 7-8) vary considerably, especially in the range of 0 to 3 kHz. The smooth appearance of figures 4 and 5 is changed to a spiky form as resonances in the response of the block-press system appear. Again, this is typical of all tests where static loads were applied. As loads were increased, these resonances

---

[3]Reference to specific trade names is made for identification only and does not imply endorsement by the Bureau of Mines.
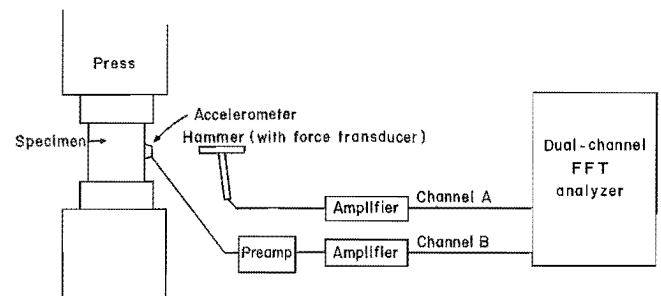

FIGURE 2. - Block diagram of laboratory experiments performed to determine the resonant shifts in stressed rock samples.

shifted to higher frequencies at a rate of approximately 100 Hz per 8.9 kN. The exact frequencies at which resonances appear depend on the block size, shape, and integrity, and the properties of the press. However, the general shift toward higher frequencies with increasing stress (corresponding to increasing terms of the stiffness matrix) agrees with theoretical and model studies presented by Allison and Lama (10). In a mine opening, increasing stress on a slab could be thought of as increasing the coupling between that rock and its surroundings, and hence increasing its stability. These laboratory tests imply that a series of measurements showing a systematic downward shift of resonant frequencies would indicate decreasing coupling between a slab and surrounding rock and so warn of increasing instability.

While this shift of resonant frequencies is measurable and would supply at least a crude measure of rock stability, this line of investigation was abandoned. The reason for this is that two sets of measurements at different times would be required to obtain a measure of rock decoupling. A first measurement would be required to establish a baseline and a second to measure the degradation of the block condition with time. Hence an immediate determination of rock stability would not seem practical using the property of shifting resonances.

FIELD TESTING

Since laboratory testing confirmed the theoretical and empirical results of Allison and Lama (10) and Summerfield
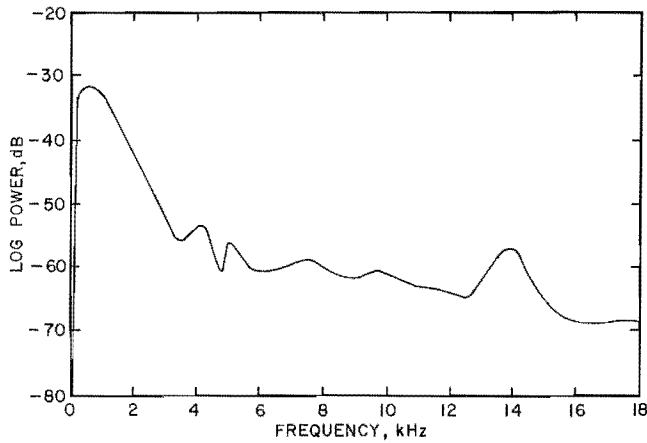
FIGURE 3. - Power spectrum of input forcing function applied to an oil shale sample with O N applied force.
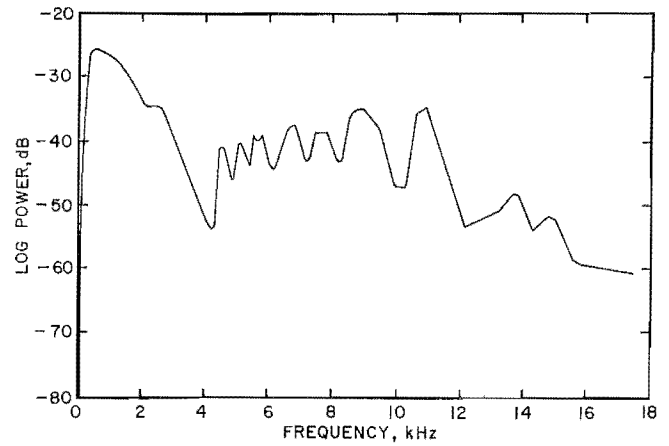
FIGURE 4. - Power spectrum of sample acceleration caused by the input forcing function of figure 2. Sample had O N applied force.
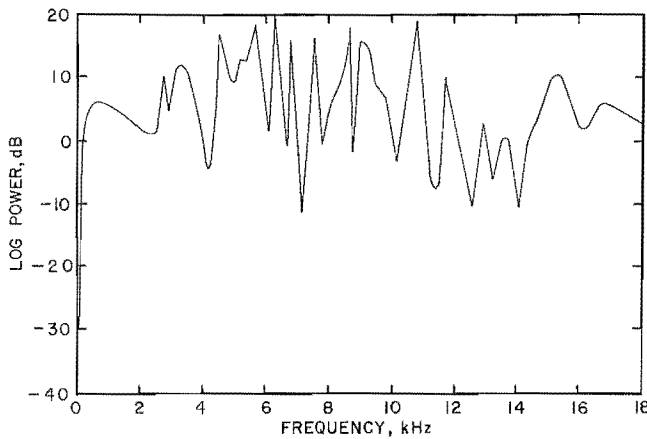
FIGURE 5. - Inertance function (output acceleration divided by input force) computed for the spectra in figures 3 and 4.
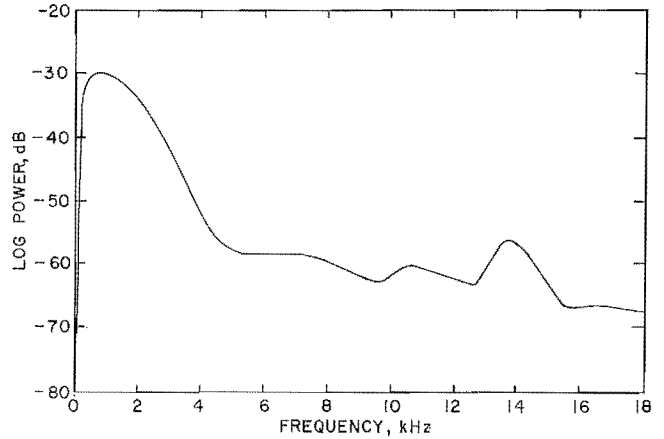
FIGURE 6. - Power spectrum of input forcing function applied to an oil shale sample with 17.8 kN applied force. Note the similarity to figure 3.
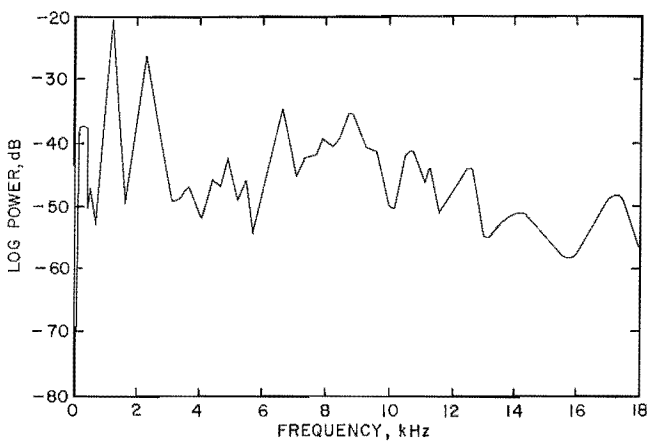
FIGURE 7. - Power spectrum of sample acceleration caused by the input forcing function of figure 6. Sample had 17.8 kN applied force. In contrast to figure 4, this spectrum is broken into line spectra characteristic of resonant peaks and nodes.
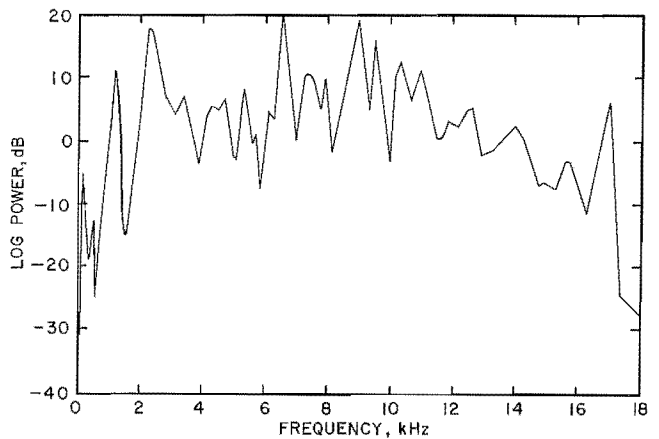
FIGURE 8. - Inertance function computed for the force and acceleration spectra of figures 6 and 7.

(5), that the mechanical resonances of rock slabs change with the degree of coupling, field tests were made to measure the acoustic response of slabs in a mine environment. A 1.8-m scaling bar of 318-mm steel tube with a chisel point was manufactured for use as the energy source in these experiments. A Dunegan/Endevco 2219E accelerometer was mounted on the chisel point to measure input acceleration. Its output was sent into an amplifier (-10 dB) and one channel of a cassette data recorder. This tape deck recorded frequencies from nearly DC to 5,000 Hz. Another 2219E accelerometer was held with a spring-loaded pole against the slab to be tested. Coupling was made with a heavy-viscosity coupling gel. The output from this accelerometer was fed to another amplifier (+30 dB) and into the tape deck (fig. 9). Each rock was lightly tapped a total of 30 to 40 times at a distance of 15 to 30 cm from the detector phone. Tapes were returned to the laboratory and played through an FFT analyzer. Power spectra of the bar and rock responses for each of the 30 to 40 impacts were averaged, and the transfer function between the averaged spectra was computed. Slabs were classed as drummy or solid based on judgments made by an experienced miner at the time of testing.

Figure 10 shows a typical power spectrum of the scaling bar. Bar responses were extremely consistent from test to test and showed little or no variation with changing rock stability. Thus, it is apparent that simple integration of a detection system onto existing scaling

bars is not viable. The bar response is dominated by its own resonances and shows no indication of rock condition. Figures 11 and 12 are power spectra of two roof slabs in the Colorado School of Mines (CSM) experimental mine, Idaho Springs, CO. A very definite, diagnostic difference occurs between the power spectrum of a drummy slab in figure 11 and that of a solid block in figure 12. While exact resonances and nodes are dependent on individual slabs, the dramatic decrease in

FIGURE 10. - Power spectrum showing resonances of the scaling bar used in field experiments.

FIGURE 11. - Averaged power spectrum of response of a drummy slab in the CSM experimental mine to impact testing.

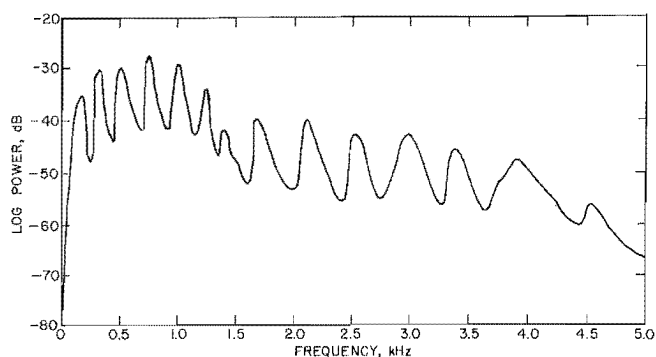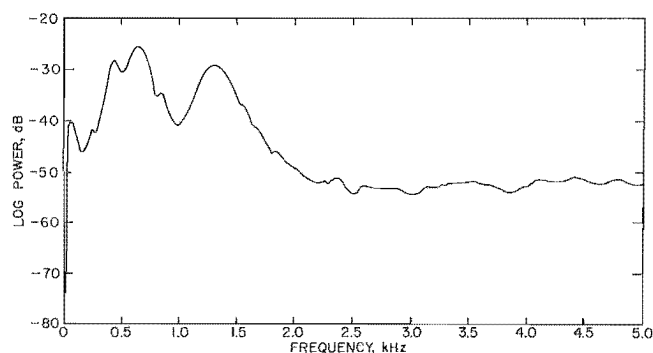
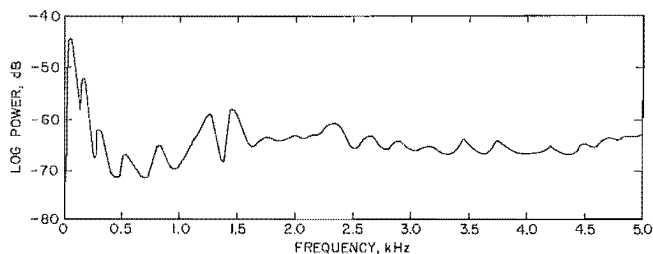FIGURE 9. - Block diagram of experimental setup for field experiments.

FIGURE 12. - Averaged power spectrum of response of a solid slab in the CSM experimental mine to impact testing.

energy present in the 0.2- to 1-kHz range between a solid and drummy block was observed to be a general characteristic. This behavior is consistent with elastic theory. A completely solid rock could be viewed as approaching a half-space. As such, when it is impacted, energy would be radiated away without encountering any acoustic discontinuities. The energy detected would generally be lower in amplitude, and no resonances would be set up. The same block held in place very loosely would approach the other extreme, a free body, and would have all the input energy confined to the block. In this case, numerous resonances (depending on the block geometry and input forcing function) will be excited and lower frequency, higher amplitude vibrations will dominate. Increasing coupling will form a transition between these two extremes.

To test the universality of this spectral property, experiments were performed in the AMAX Henderson Mine (molybdenum), Empire, CO, and the CSM experimental mine (both hard-rock environments), and the Mid-Continent Resources L. S. Wood #3 Mine (a coal mine), Redstone, CO. Summarized results of these tests are shown in figures 13 to 15. Data were collected and analyzed in an identical manner for all mines. Spectra shown are smoothed to show general behavior. The most striking contrast between solid and drummy rocks is seen in the range of 0.2 to 1 kHz, where differences of up to 15 dB are evident. The variation in power spectra between drummy and solid rocks is evident in data from all mines even though they consist of widely varying rock types. From these results it appears that a measurement of the energy content between 0.2 and 1 kHz in the accelerometer signal generated from an impact can provide a

FIGURE 13. - Summary of power spectra computed for solid and drummy rocks in the CSM experimental mine. Spectra are smoothed to show the general behavior of the block types.
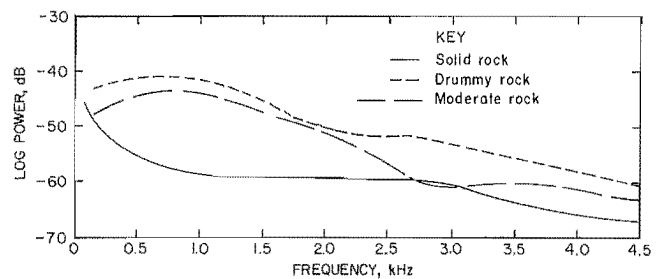
FIGURE 14. - Summary of power spectra computed for slabs tested in the AMAX Henderson Mine. Spectra are smoothed to show general behavior of the block types.
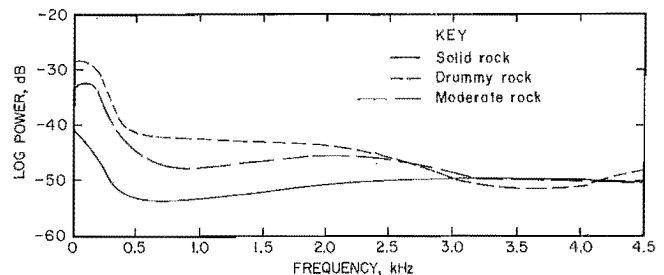
FIGURE 15. - Summary of power spectra computed for slabs tested in the Mid-Continent Resources L.S. Wood #3 Mine. Spectra are smoothed to show general behavior of the block types.

rapid, accurate diagnostic measure of roof stability.

INSTRUMENTATION DESIGN

CIRCUIT DESIGN

The different spectral properties of solid and drummy rock as seen in figures 13 to 15 provide a means of distinguishing the rock types based on their impact response. Howe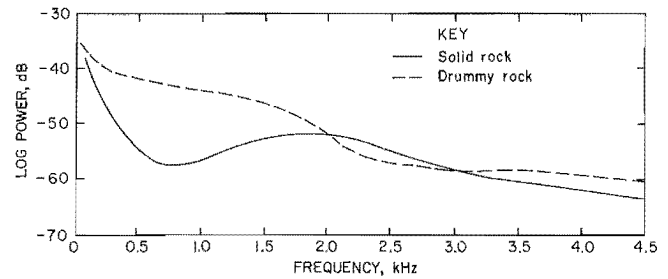ver, to make use of this property, a means to analyze the power spectra without sophisticated Fourier analysis equipment is required. To accomplish this, an electronics prototype based on the block diagram of figure 16 was designed and constructed.
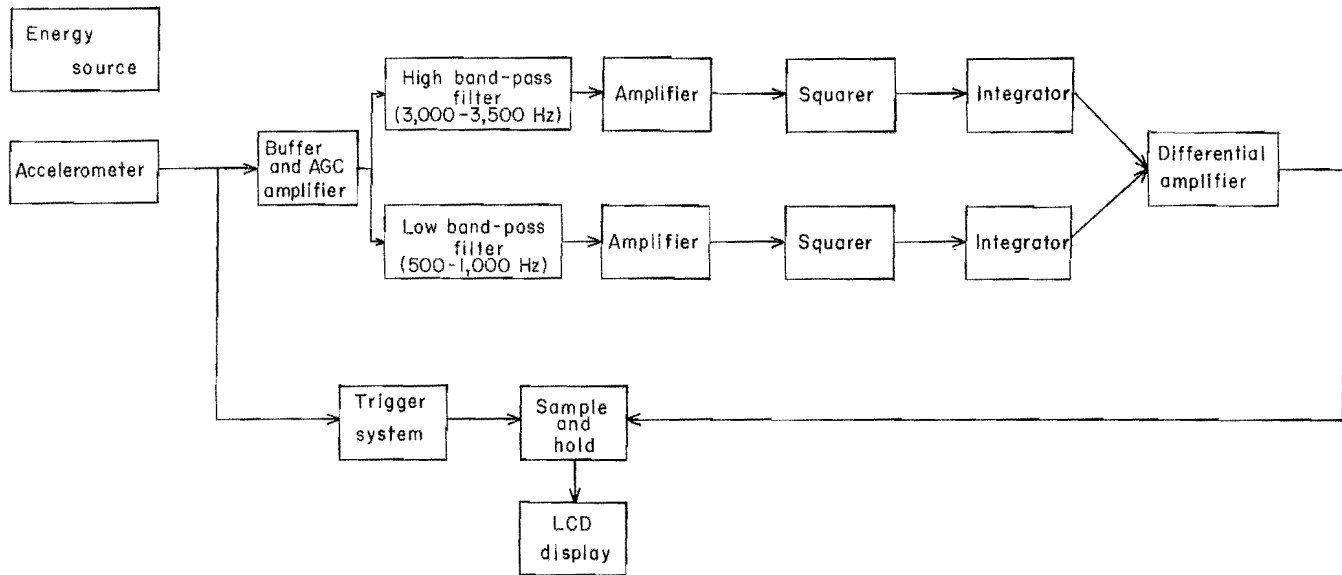
FIGURE 16. - Block diagram of electronics package designed to use the spectral differences between impacted solid and drummy rocks to obtain a measure of rock stability.

The general operation of the circuit is as follows. A signal detected by an accelerometer (Dunegan/Endevco 2219E) held against the rock is input to a buffer and automatic gain control (AGC) amplifier. The AGC amplification can be as high as +40 dB but is lowered with larger input amplitudes automatically to prevent clipping and distortion of the input waveform. This amplified signal is then split into two frequency bands: a low band where most of the resonant energy of drummy rocks is concentrated and a high band where power spectra from drummy and solid rocks are roughly equivalent. These filters are four-pole Chebyshev band-pass filters with 0.5 dB ripple in their passbands. The low band-pass filter was designed with Q = 2.5 and a passband of 500 to 1,000 Hz. A passband of 3,000 to 3,500 Hz and Q = 10 were used in the high band filter. These filter outputs are then amplified, squared, and integrated. These operations provide a measure of the power contained in the two frequency bands. The integrators are turned on by a one-shot pulse from the trigger system so that integration occurs only after the rock has been impacted. The two integrated signals are then fed to a differential amplifier. This device

outputs a voltage proportional to the difference in power contained in the two frequency bands. It is this output that provides a measure of rock stability. This voltage is finally input to a sample-and-hold circuit and displayed on a low-power liquid crystal (LCD). By utilizing an AGC and a differential amplifier, the effect of variations in impact force from blow to blow is minimized. Referring to figures 13 to 15, the spectral differences between drummy and solid rocks disappear at higher frequencies, except for a DC shift dependent on the overall impact energy. The power content at higher frequencies provides a baseline against which to compare the low-frequency energy and eliminate the effect of impact differences.

The difference in power in the low- and high-frequency bands thus gives a number, minimizing the effect of overall blow energy, which provides a measure of block stability. A large number indicates a dominance of low-frequency energy. This shows that the block is relatively more decoupled and unstable. A solid block, on the other hand, has roughly equal energy across the spectrum (as seen in figure 12) and so will have a small difference voltage.

As the signal is input to the AGC it is also split off to control a trigger circuit. This half of the circuit is used to turn on the integrators and sample-and-hold system only when an impact is detected. The signal is amplified, full-wave rectified, and amplified again to the point of clipping. The positive going impulse of this essentially square wave is used to trigger a dual one-shot. This in turn controls analog switches that turn the integrators and sample-and-hold system on and off. Two time constants are used with the dual one-shot. This allows the integrators to be on longer than the sample phase of the sample and hold. The sample and hold is thus prevented from possibly holding on a transient caused by the integrators' turning off at the end of their cycle. As designed, the electronics requires approximately 50 mA quiescent current and operates from one 9-V and two 12.6-V batteries.

TEST RESULTS

Once the design was finalized and the circuit debugged, tests were performed on previously collected data tapes and new field data. New data were collected in the CSM experimental mine, the Dutch Creek #1 Mine (coal), Redstone, CO, and the Bureau's Twilight Mine (uranium), Uravan, CO. Data collection was identical to that illustrated in figure 9, except that the accelerometer output was split off before the amplifier and input to the electronics prototype. A series of 30 to 40 impacts was made on each block. Instrument readings from each block in the field were averaged, and a standard deviation was calculated. In addition, tapes were returned to the laboratory and averaged power spectra computed. Data on tapes already collected were played back through an attenuator to remove gain applied at the time of collection and then into the prototype. No significant differences were seen between readings made directly in the field and those obtained by playing tapes of the same tests through the electronics in the laboratory. Figures 17 through 20 show averaged readings and standard deviations versus approximate block volume for both field tests and tapes analyzed in the laboratory. These plots show a definite difference in readings between what were classed as stable and unstable blocks. Solid blocks had average values below a device reading of 5 and maximum standard deviations of 5. Moderate blocks had slightly higher averages and larger scatter, and generally, drummy rocks had the highest readings and largest scatter. Figure 21 is a histogram of frequency versus average device reading for each rock type. From this, the distribution of rock type with device reading can be seen and the general increase in readings with decreased stability noted. A question that arose during field testing was whether the low-frequency enhancement could be seen in blocks of increasing size. Rough estimates of block size were made for each test and volumes computed. Figures 17 to 20 show no systematic change in device reading with increasing block size. Therefore, it would appear that examination of spectral differences is a valid technique to judge rock stability for the size range tested here.

A comparison of figures 17 and 18 with 19 and 20 reveals a reduction in the separation of average readings between solid and drummy rocks. Figures 17 and 18 are results from the hard-rock CSM and Henderson Mines, and figures 19 and 20 are from the shales and sandstone of the L. S. Wood #3, Dutch Creek #1, and Twilight Mines. Assuming that this decrease of separation is a reflection of rock properties and not equipment malfunction, this behavior may possibly be explained by the introduction of damping. As shown in figure 1 and equations 11 and 12, a decrease in Q corresponds to an increase in damping (ζ) and a reduction in amplitude and broadening of resonant peaks. Assuming major resonances occur in the low-frequency band of the filters, any reduction in their amplitude will decrease the difference between the power contained in the two frequency bands. This will reduce the device readings for

FIGURE 17. - Average device readings and standard
deviations for tests performed in the CSM experimental
mine.
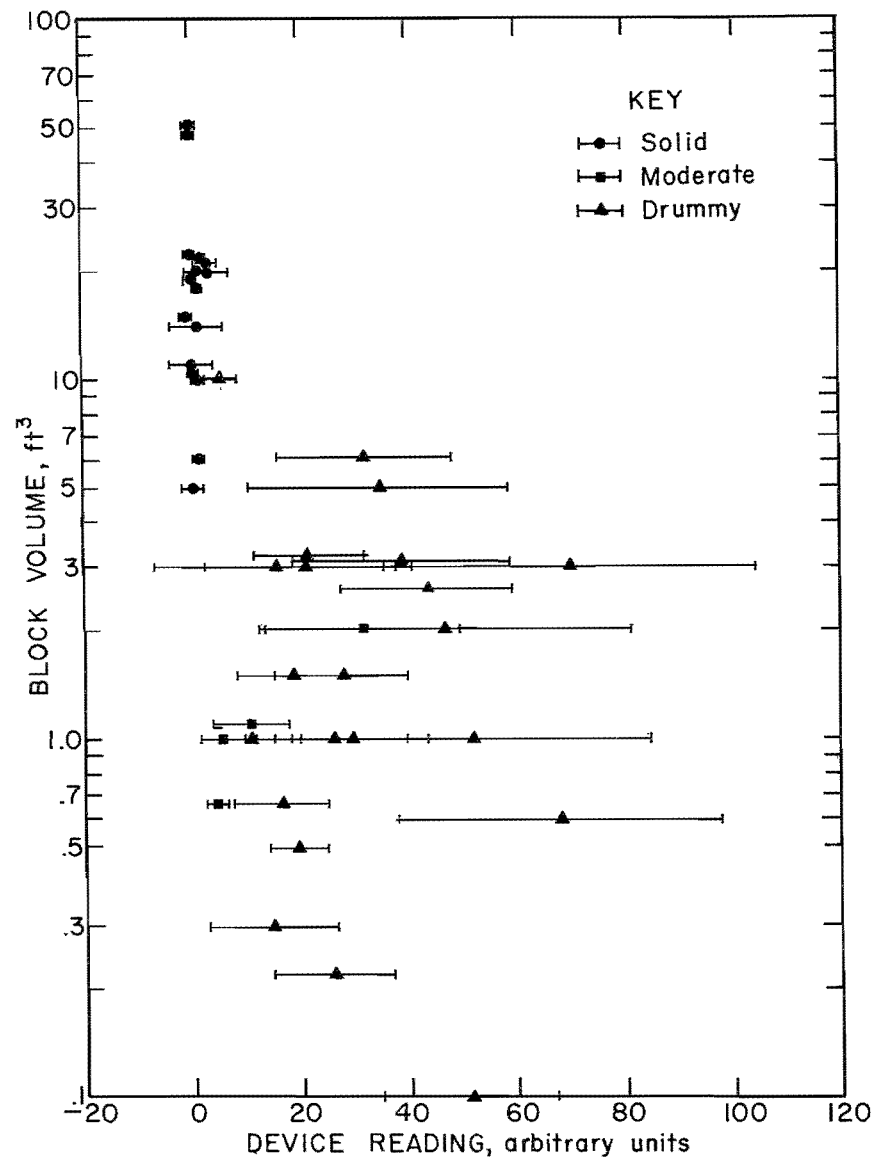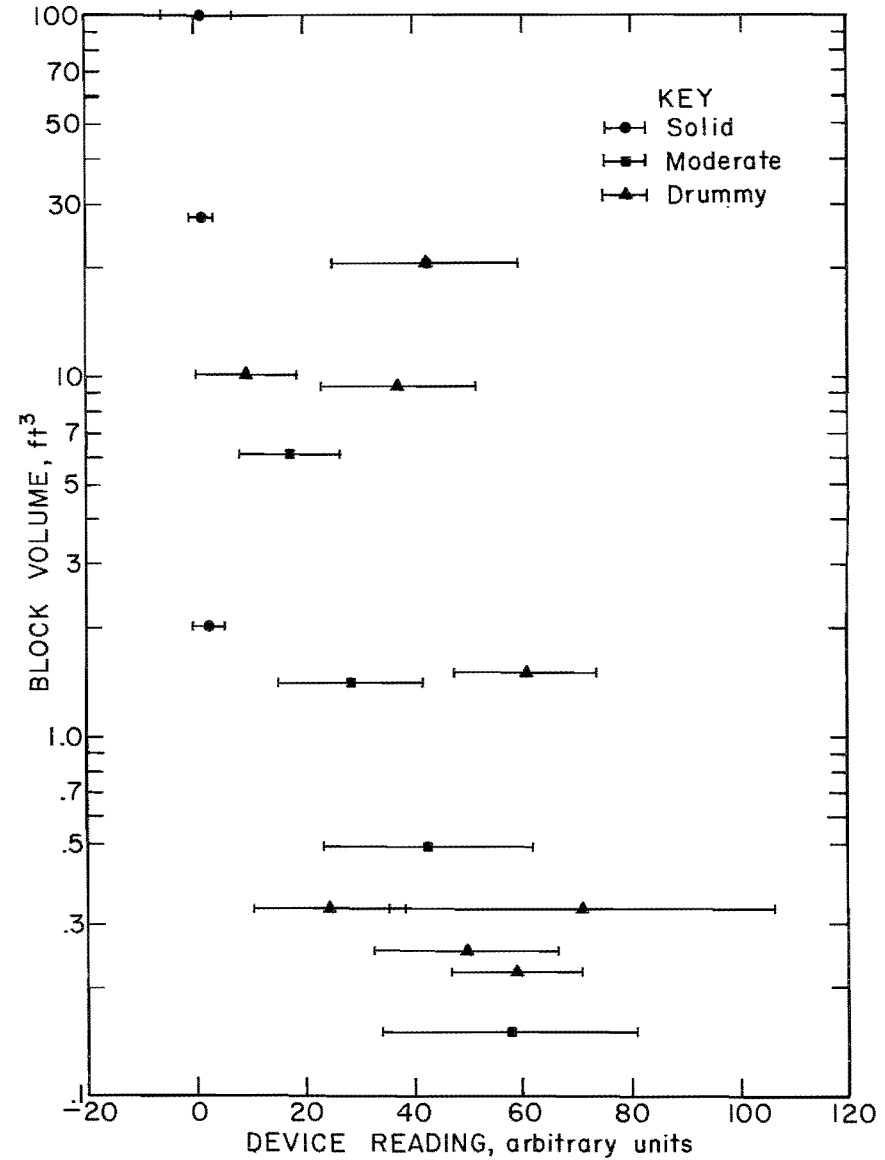
FIGURE 18. - Average device readings and standard
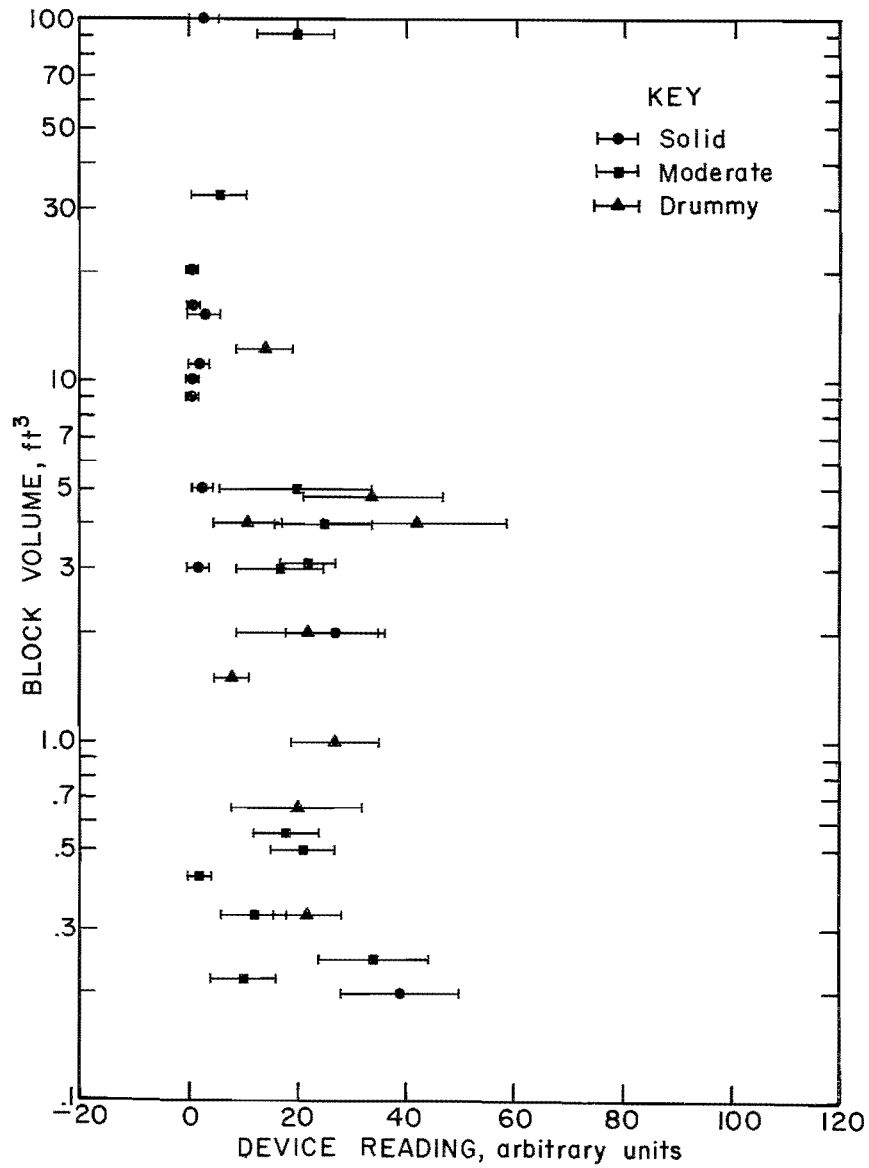deviations for tests performed in the AMAX Henderson
Mine.

FIGURE 19. - Average device readings and standard deviations for tests performed in the Bureau's Twilight Mine.
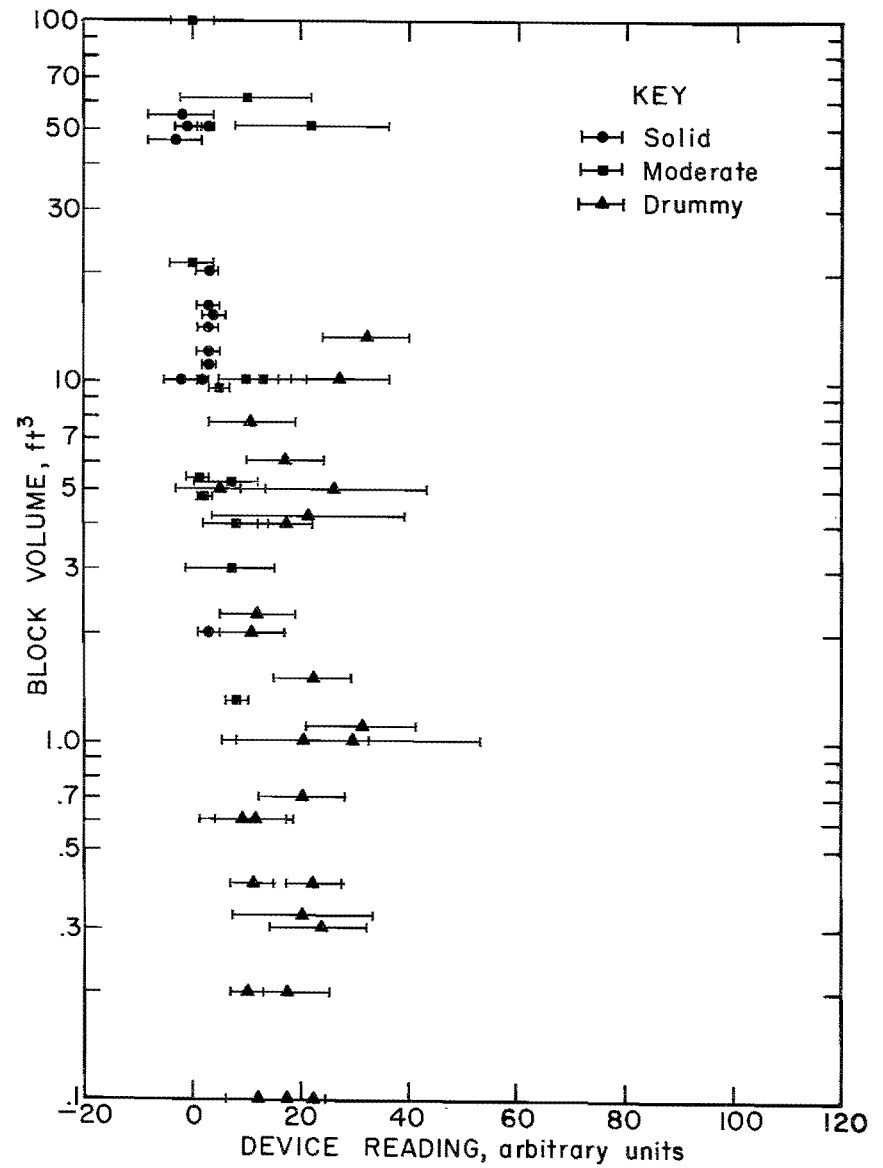

FIGURE 20. - Average device readings and standard deviations for tests performed in the Mid-Continent Resources Dutch Creek #1 and L. S. Wood #3 Mines.
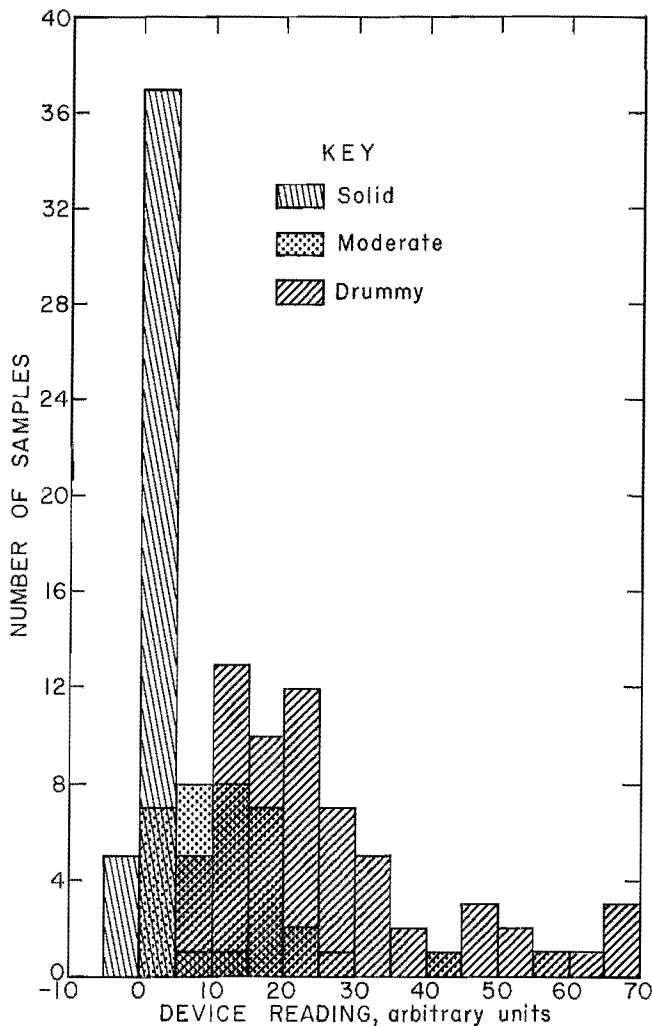
14

FIGURE 21. - Histogram of the frequency of occurrence versus device reading for solid, moderate, and drummy classed slabs. This figure includes readings from all of the different mines tested.

drummy rocks and force their values to appear more like solid rocks. White (11) lists values of Q of 50 to 70 for shales and 100 to 200 for granites. Therefore, the increased damping of the softer shales and sandstone may account for the reduction in separation seen in figures 19 and 20. As a possible solution to this problem, field tapes were replayed after the gain of the differential amplifier was doubled. Results are shown in figures 22 to 25. Obviously, separation was increased, but at the expense of an increase in data scatter. For very soft-rock mines this tradeoff may be required for the technique to be viable.

The relatively large amount of scatter present in the data of figures 17 to 20 is undesirable but may be unavoidable. This scatter has three most probable causes. The first is variation in impact spectra from one blow to the next. Summerfield (5) noted that most of his spectra varied in overall amplitude but not in frequency content. This general behavior was also observed in this study, but minor changes may be enough to cause variance in detected waveforms. Secondly, for all tests, a scaling bar with a chisel point was used as an energy source. Because of the geometry of the point, impacts may come from corners or a flat edge. This will cause some variation in the input spectra. To test this hypothesis, a sounding stick with a round machined steel head was obtained from the Mine Safety and Health Administration. A cursory series of tests was made to compare results from the sounding stick and chisel-pointed scaling bar. Some reduction in scatter was seen, but nothing significant. Finally, a large portion of the scatter is due to the manner in which the data were collected. For each test, three sets of 10 taps were made at points about the same radial distance from the detector but at approximately 120° intervals around it. Readings for each location were usually quite consistent, but this was not necessarily the case between sets. To obtain the averages shown in the figures, all readings were averaged together. This adds considerably to data scatter. The variation of readings between impact points would seem to indicate that readings from any set are a reflection of very local rock conditions in the immediate area of the impact point and accelerometer.

DESIGN IMPROVEMENTS

Although the technique described here is workable as a method to discriminate between solid and drummy blocks, modifications may be made to improve overall performance. Without changing the basic circuit design, power consumption may be significantly reduced by replacing the higher power integrated circuits (notably

FIGURE 22. - Equivalent figure to figure 17 for the CSM experimental mine, except that gain on the differential amplifier was doubled.

FIGURE 23. - Equivalent figure to figure 18 for the AMAX Henderson Mine, except that gain on the differential amplifier was doubled.
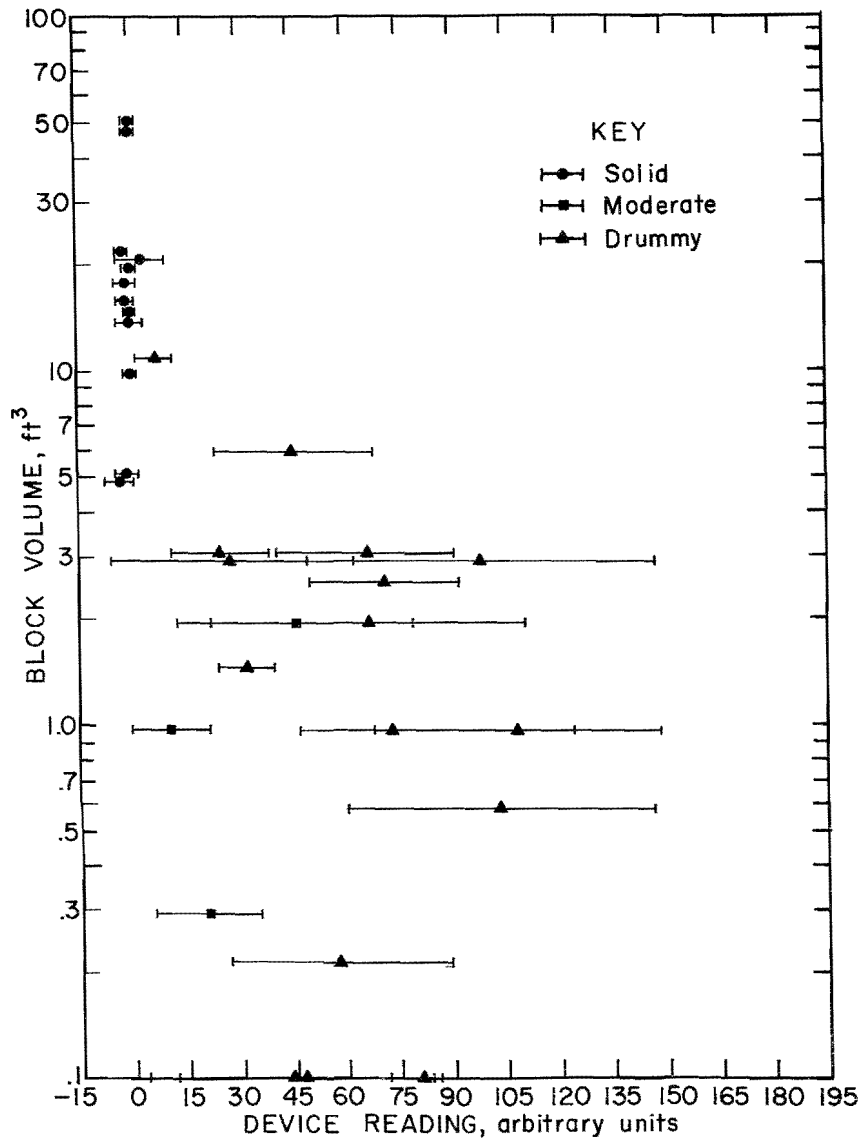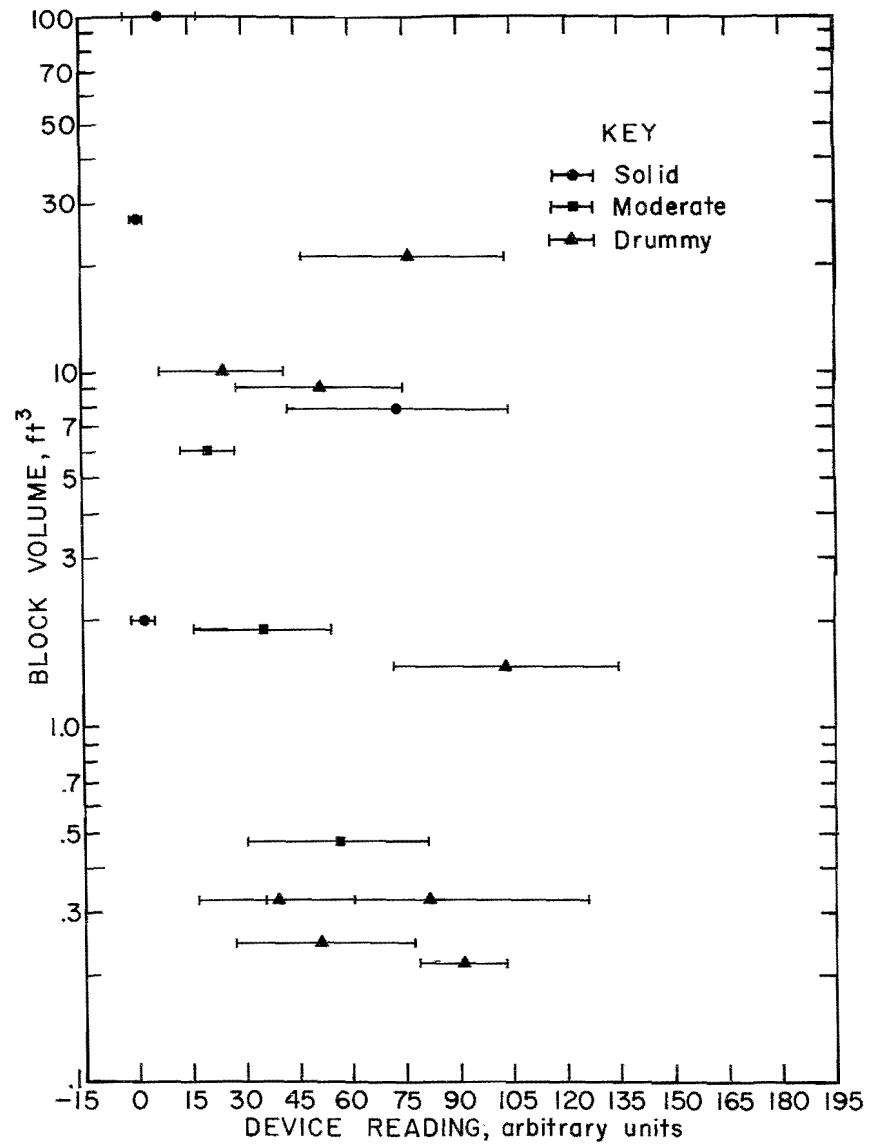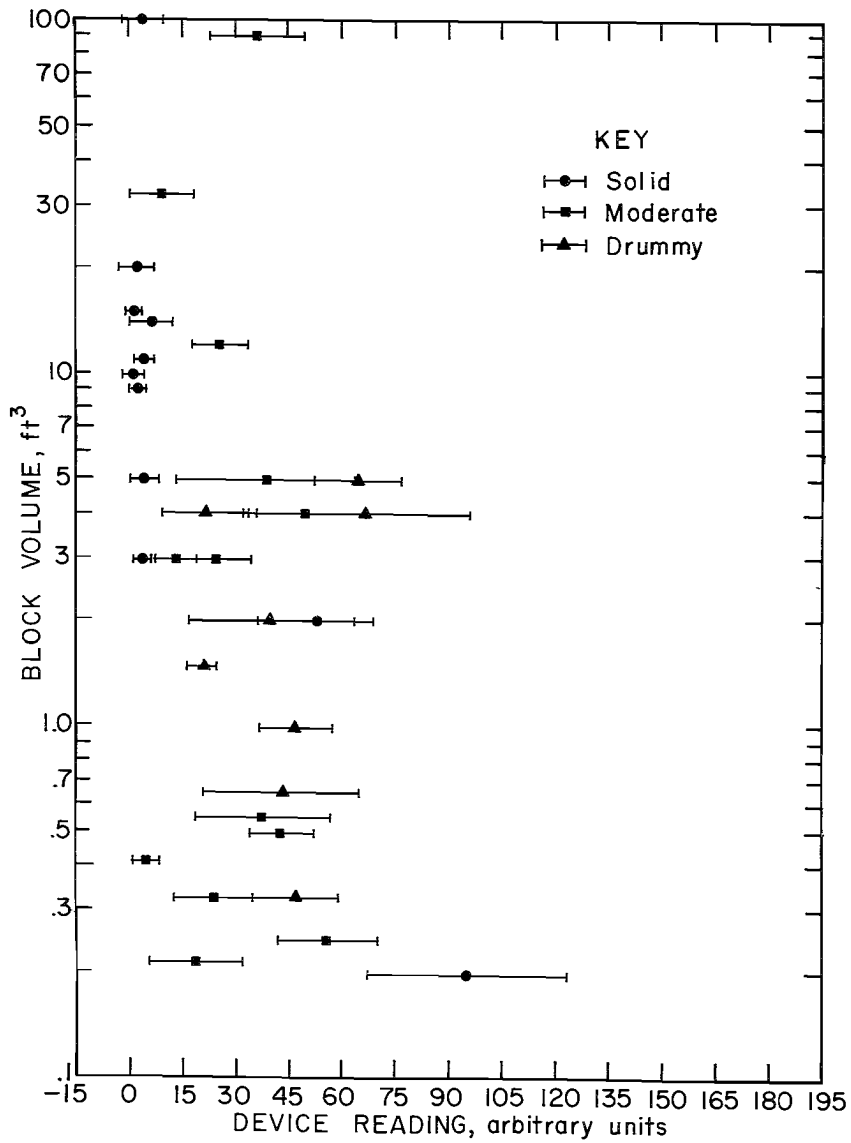
FIGURE 24. - Equivalent figure to figure 19 for the Bureau's Twilight Mine, except that gain on the differential amplifier was doubled.
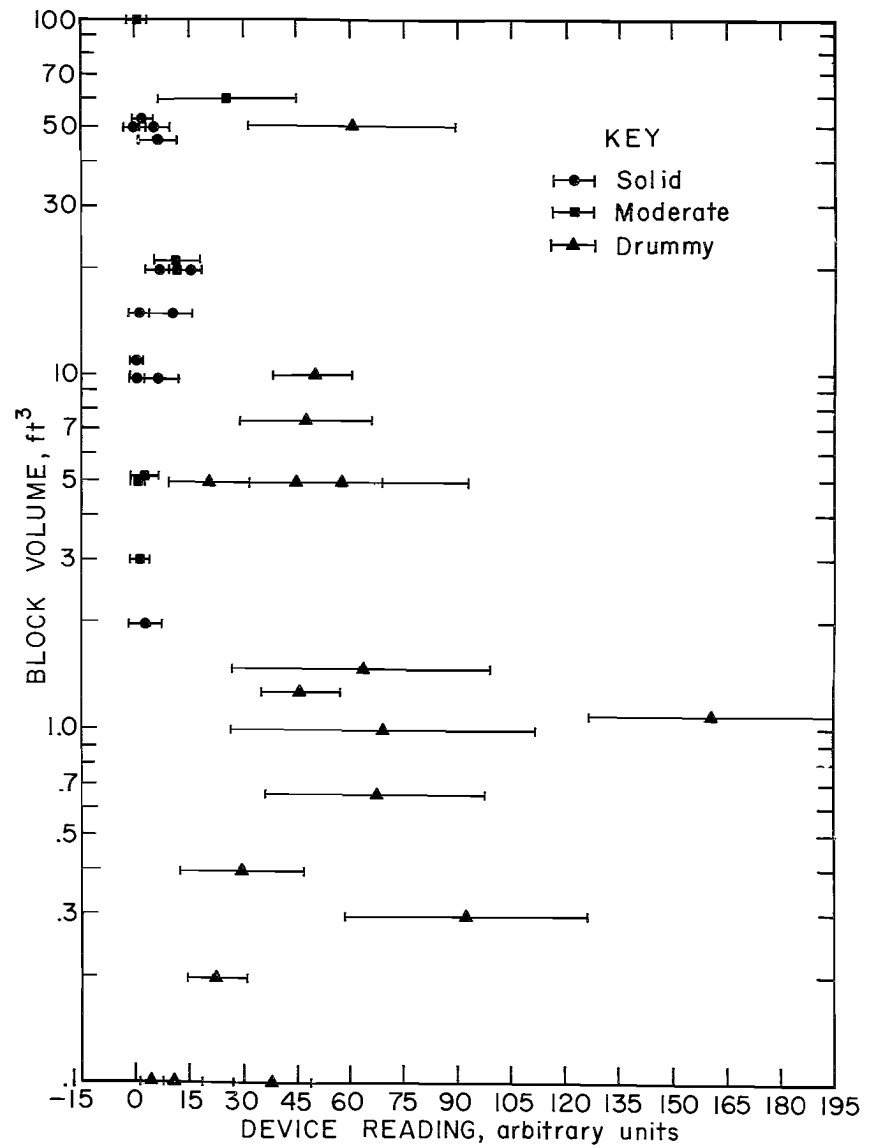
FIGURE 25. - Equivalent figure to figure 20 for the Dutch Creek #1 and L. S. Wood #3 Mines, except that gain on the differential amplifier was doubled

the Burr-Brown filters). Filters designed with discrete components and micropower operational amplifiers might allow a reduction of power consumption by half. The device may then be operated using two 9-V transistor batteries, rather than the one 9-V and two 12.6-V batteries used now. This would also allow a reduction in size. The prototype is currently housed in a 21.5- by 19- by 7.6-cm enclosure. Mounting of components on a printed circuit board and a reduction in battery size would increase convenience. Although a great improvement in data scatter was not realized by using a rounded sounding stick, it is felt this sort of impactor would provide a more stable input waveform than the chisel point from simply geometric factors.

A major change and improvement could be made by shifting the currently used analog signal processing scheme to digital. All filtering, spectral computation, differences, and displays could be performed from a microprocessor chip base. This would increase stability and reliability and eliminate many of the problems inherent in analog signal processing.

It should be noted that the technique has fundamental limitations. The most important of these is that it does not work well when the detector is mounted on the edge of a plate. Modes excited when the impact and detection points are on an edge do not show diagnostic spectral differences. Most accurate readings are obtained when the detector can sense drumhead modes in a plate. Secondly, if a rock being tested has two free faces, such as a point of rock jutting into a drift, low-frequency resonances will be set up between the two faces. This results in spectra that resemble those of drummy slabs, even if the rock tested is quite solid. Resonances used by this technique are set up between the rock's free face and the first major crack. Thus, no information is available on rock conditions beyond the first major parting.

CONCLUSIONS

Laboratory and field experiments have confirmed theoretical results showing that spectral differences exist in the vibrations of impacted solid and drummy rocks. Although not viable as a fast field test, laboratory experiments have shown that as stress is applied to a rock, its resonances will increase in frequency. In blocks tested, this increase was approximately 100 Hz for each 8.9 kN of applied force. This suggests that detached blocks in a mine environment should have a preponderance of low-frequency resonances as compared with solid rocks. Field tests in five mines (two hard rock, two coal, and one sandstone) confirmed this, as drummy slabs demonstrated a diagnostic enhancement in the low-frequency end of the acceleration power spectrum resulting from impacts. Although the exact resonant frequencies depend on block shape, physical conditions, composition, and size, and mode of excitation, energy content in the 200- to 1,000-Hz frequency range was greater in drummy rocks than in solid ones. This spectral difference disappeared as frequency increased. Therefore, the technique of computing the difference in energy between a low- and high-frequency band was used to measure rock stability.

To avoid the need for complex spectral analysis techniques and equipment in the field, an electronics prototype was designed and constructed. This instrument performs an analogous function to a Fourier spectrum analyzer. It will detect a signal, compute the difference in power between two frequency bands, and display the results. Once the prototype was completed, it was tested both in mine environments and with data tapes in the laboratory. Based on instrument readings, a decision could be made as to the stability or drumminess of each rock tested. This technique appears to operate best in hard-rock mines where the rocks generally have a high Q or low damping. Increased damping (as seen in coal mines) results in lowering the amplitude of resonant peaks. This degrades the ability of the instrument to discriminate between stable

18

and unstable rocks. This shortfall may be partially overcome by increasing the gain in the difference computation.

Advantages of this system are that it requires no special interpretation, can be used on any rock type, and may be used under conditions where a normal sounding by ear is not accurate or even possible. Impacts used to obtain readings are much less energetic than those normally made. Finally, this technique holds the possibility of being performed remotely, thus removing the miner from the immediate area of hazardous roof.

REFERENCES

1. Heim, M. H. Analysis of Falls of Rib, Roof, and Face Accidents in Underground Coal Mines, 1977-1979. MSHA, Rep. Analysis, 1980, 16 pp.

2. Galloway, C. Tables for Falls of Roof, Face, or Rib Fatalities in Underground Coal Mines, 1980. MSHA, Rep. Analysis, 1981, 14 pp.

3. ____. Nonfatal Injuries From Falls of Roof, Face, or Rib (Includes Pressure Bumps or Bursts) in Underground Coal Mines, 1980. MSHA, Rep. Analysis, 1981, 9 pp.

4. ____. Nonfatal Injuries From Falls of Roof, Face, or Rib (Includes Pressure Bumps or Bursts) in Underground Coal Mines, 1979. MSHA, Rep. Analysis, 1980, 9 pp.

5. Summerfield, P. N. A Study of the Air and Rock Vibrations Produced by Impact Testing of Mine Roof. BuMines RI 5251, 1956, 37 pp.

6. Faire Equipe. Vibrometre de Toit (Roof Vibrometer). No. 67, 1974, pp. 213-214.

7. Palmer, E. P., and J. B. Czirr. Spectral Analysis of Coal Mine Roof Vibrations. Min. Eng. (Littleton, CO), v. 34, No. 10, Oct. 1982, pp. 1477-1479.

8. Ewing, W. M., W. S. Jardetzky, and F. Press. Elastic Waves in Layered Media. McGraw-Hill, 1957, 380 pp.

9. Siggins, A., and J. R. Enever. A Laboratory Simulation of the Influence of Defects on the Dynamic Response of a Rectangular Mine Opening. Paper in proceedings of the 4th Congress, International Society for Rock Mechanics (Montreux, Switzerland, Sept. 2-8, 1979). A. A. Balkema, Rotterdam, Netherlands, v. 1, 1979, pp. 293-299.

10. Allison, H., and R. D. Lama. Low Frequency Sounding Technique for Predicting Progressive Failure of Rock. Rock Mech., v. 12, 1979, pp. 79-97.

11. White, J. E. Seismic Waves: Radiation, Transmission, and Attenuation. McGraw-Hill, 1965, 302 pp.

12. Seirig, A. Mechanical Systems Analysis. International Textbook Co., Scranton, PA, 1969, 596 pp.

APPENDIX A.--CIRCUIT DIAGRAM

Figure A-1 is a block diagram of the current circuit prototype. This circuit has been constructed on a wire-wrap board approximately 15 by 10 cm. A parts list is given in table A-1.

Table A-2 lists the function of each of the integrated circuit devices listed in table A-1 along with their use according to the block diagram given in figure 16 in the main text.

TABLE A-1 - Component list for prototype

Component	Quantity	Component	Quantity
Analog Devices AD534KH.........	2	3 kΩ (10%, 1/4 W)...............	1
Burr-Brown UAF-41..............	4	5.1 kΩ (10%, 1/4 W).............	9
Intersil ICL7106 Ev/Kit........	1	6.8 kΩ (10%, 1/4 W).............	2
National LF442CN...............	6	10 kΩ (10%, 1/4 W)..............	14
National LM13600AN.............	1	15 kΩ (10%, 1/4 W)..............	2
National 13201N................	1	20 kΩ (10%, 1/4 W)..............	1
National MM74C221..............	1	27 kΩ (10%, 1/4 W)..............	2
2N2222A........................	2	47 kΩ (10%, 1/4 W)..............	2
1N914..........................	1	51 kΩ (10%, 1/4 W)..............	2
8200 pF.......................	6	82 kΩ (10%, 1/4 W)..............	2
0.0033 μF......................	1	100 kΩ (10%, 1/4 W).............	2
0.22 μF (ceramic)..............	2	150 kΩ (10%, 1/4 W).............	1
0.68 μF (electrolytic).........	2	240 kΩ (10%, 1/4 W).............	1
1 μF (electrolytic)............	3	470 kΩ (10%, 1/4 W).............	3
1.5 μF (tantalum)..............	3	510 kΩ (10%, 1/4 W).............	1
15 μF (tantalum)...............	1	680 kΩ (10%, 1/4 W).............	1
30 μF (electrolytic)...........	1	1.0 MΩ (10%, 1/4 W).............	4
220 μF (electrolytic)..........	1	2.0 MΩ (10%, 1/4 W).............	1
10 Ω (10%, 1/4 W)..............	1	3.0 MΩ (10%, 1/4 W).............	1
33 Ω (10%, 1/4 W)..............	2	20 kΩ (potentiometer)..........	1
47 Ω (10%, 1/4 W)..............	1	50 kΩ (potentiometer)..........	1
100 Ω (10%, 1/4 W).............	3	200 kΩ (potentiometer).........	6
2 kΩ (10%, 1/4 W)..............	3	500 kΩ (potentiometer).........	5

TABLE A-2. - Integrated circuit function

| Device	Function	Circuit use
AD534KH.............	Analog multiplier....................	Squarer.
BB UAF-41...........	Universal active filter..............	Band-pass filters.
ICL7106 Ev/Kit......	Liquid crystal display...............	Readout.
LF442CN.............	Micropower operational amplifier.....	Amplifier. Rectifier. Integrators. Differential amplifier. Sample and hold.
LM13600AN...........	Transconductance amplifier...........	AGC amplifier.
13201N..............	Analog switches......................	Switch.
MM74C221............	Dual one-shot........................	Do.
2N2222A.............	NPN transistor.......................	Do.
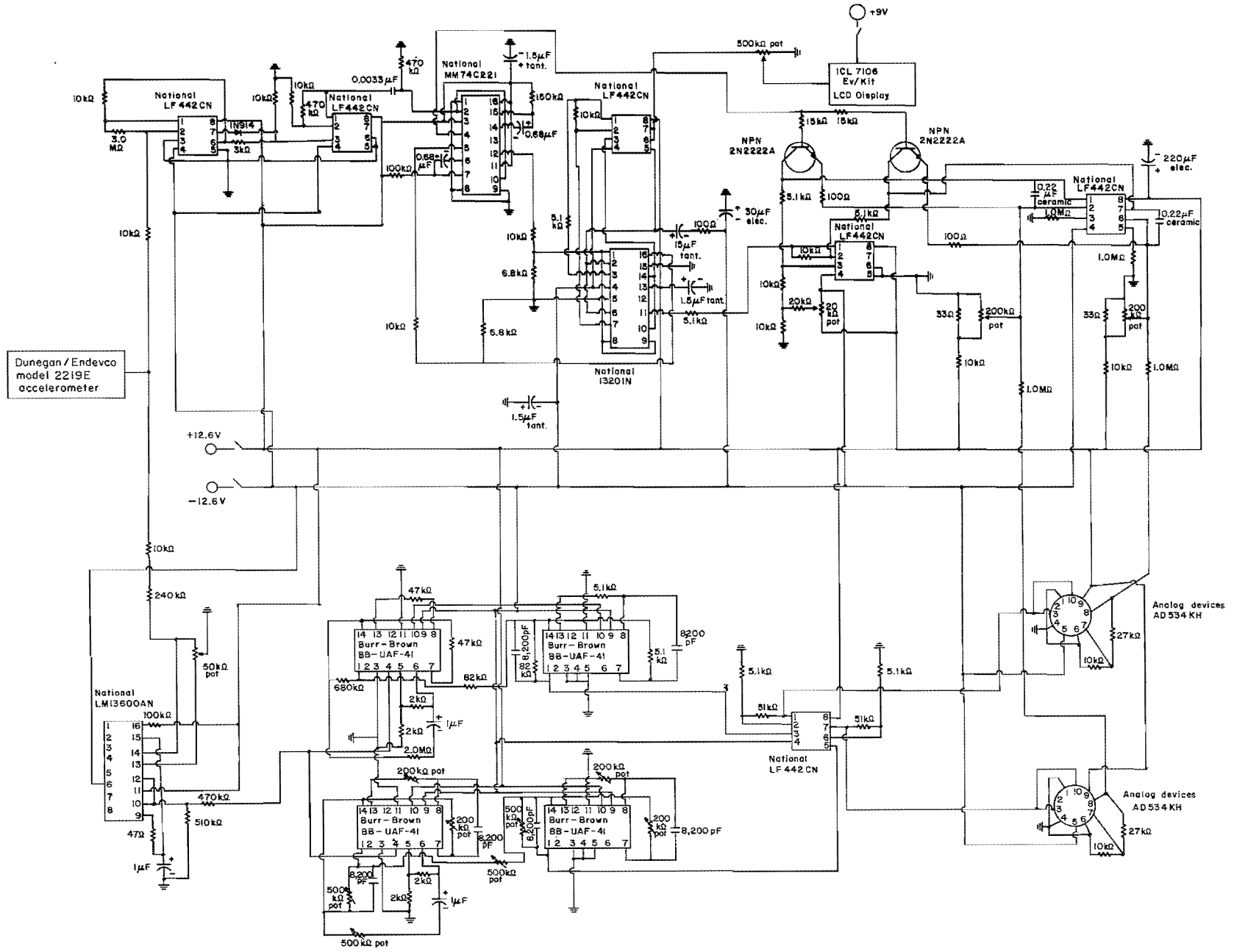
FIGURE A-1. - Schematic diagram of the current electronics circuit prototype used to measure rock slab stability based on vibrational spectrum differences.

APPENDIX B.--INSTRUMENTATION CALIBRATION

Calibration tests were conducted on the final prototype electronics by mixing 700-Hz and 3,425-Hz sine waves. The root mean square (RMS) voltage of the mixed signals was originally set at 0.0212 VRMS, and then the amplitude of one frequency component or the other was varied. This determined the relation between the device readout and the difference between the power content of the low- and high-frequency signals. This difference in power was computed in decibels and is shown as ΔdB in figure B-1. To more closely approximate the type of signal that would normally be processed, the calibration signals were pulses whose duration was varied from 10 ms in length to 70 ms. As shown in figure B-1, shorter pulse lengths tended to result in lower magnitude readouts for greater ΔdB. This effect is reduced as the pulse length is increased and probably is an effect of the analog circuitry design.
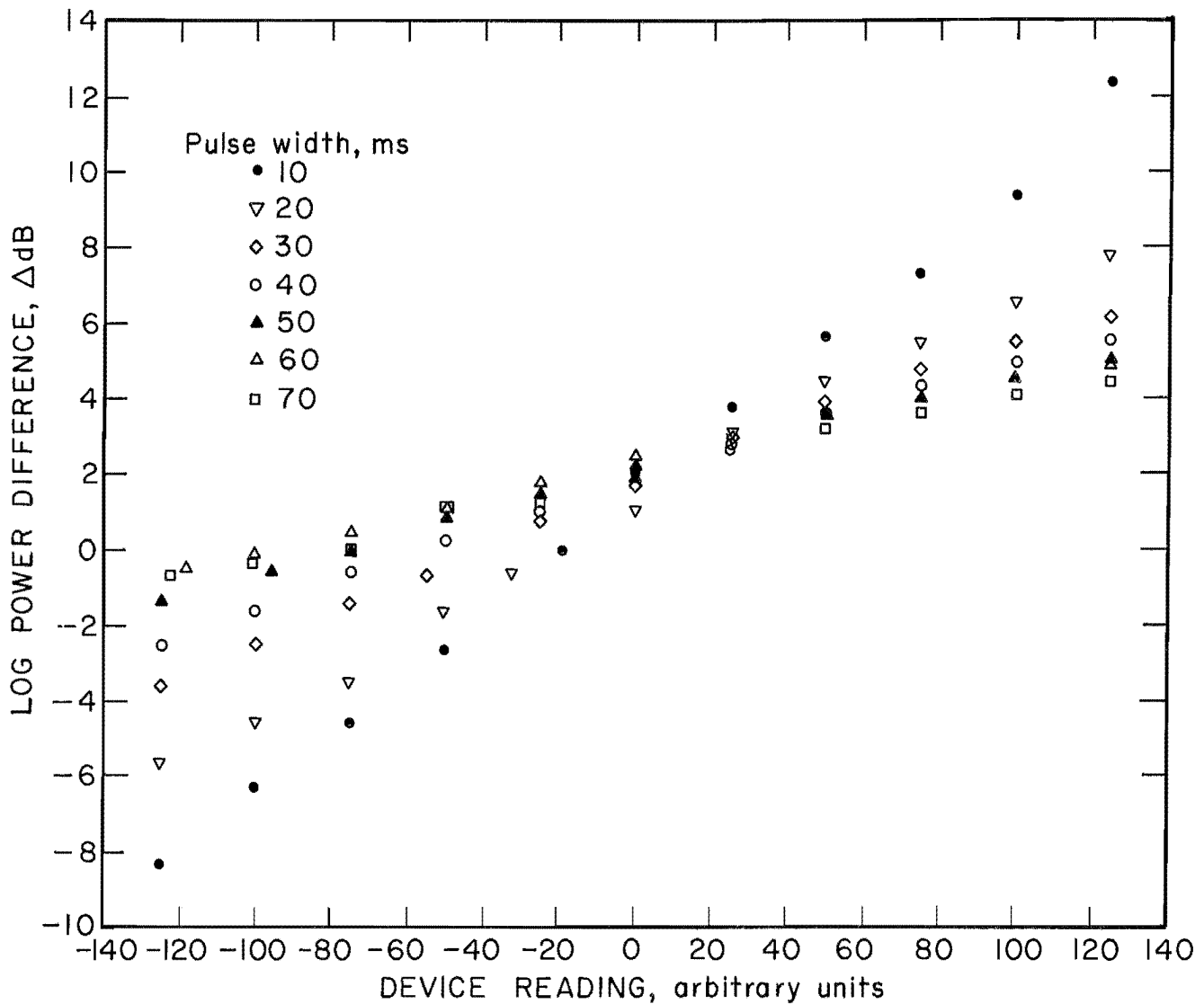

FIGURE B-1. - Calibration test on prototype. Pulse widths and amplitudes were varied to determine their relation to device reading.